This article has been accepted for inclusion in a future issue of this journal. Content is final as presented, with the exception of pagination.

Cross Evaluation of Waveform Modulation Schemes Using Postexperimental Field Data

Yukang Xue, Xiangzhao Qin, *Member, IEEE*, and Yahong Rosa Zheng, *Fellow, IEEE*

***Abstract*—This article extends the data dithering reuse (DDR) method to waveform modulation for underwater acoustic communications and enables postexperimental cross evaluation between single-carrier modulation (SCM) and orthogonal frequency-division multiplexing (OFDM). The proposed DDR method reuses the data from the original experimental scheme (OES) to evaluate a new scheme under test with different waveform modulations by adding dithering and reverse dithering, respectively, to the transmitted and received OES data. The proposed DDR method consists of three steps: 1) data block preparation; 2) waveform dithering; and 3) channel estimation and reverse dithering. OFDM signals with cyclic prefix or zero-padding guard intervals can be evaluated with the SCM of different constellation orders and vice versa. We demonstrate the effectiveness of the proposed cross-evaluation method using multiple-input multiple-output (MIMO) field measurements from the undersea 2008 Surface Processes and Acoustic Communications Experiment, compared to the original experimental data sets and existing residual prediction error (RPE)-enhanced replay simulations. The MIMO soft-decision frequency-domain Turbo equalization is used to detect both the SCM and OFDM schemes. The results confirm that the average bit error rate (BER) and the BER distribution predicted by the proposed DDR method are closer to the OES evaluation and are more robust than the RPE-enhanced replay simulation.**

***Index Terms*—Data reuse, orthogonal frequency-division multiplexing (OFDM), single-carrier modulation (SCM), underwater acoustic (UWA) communications, waveform modulation.**

I. Introduction

UNDERWATER acoustic (UWA) communication systems experience challenging underwater environments [1], which often result in unsatisfactory performance of physical layer communication systems. Although computer-generated Wide-Sense Stationary Uncorrelated Scattering channel models are widely accepted in terrestrial RF communications [2], [3], the UWA community lacks universally accepted channel models, making it difficult to effectively evaluate the performance of different algorithms using numerical simulations. The difficulties encountered in numerical simulations of acoustic communication channels include the nonlinearity and wide-sense nonstationarity of acoustic propagation, as almost all available channel models [4], [5], [6], [7] assume the wide-sense stationary property by specifying spatial–temporal correlation and the linearity by using convolution to describe the channel input and output relationship. These assumptions differ significantly from reality, resulting in the prediction of unrealistic performance of the scheme under test (SUT). Therefore, researchers in the UWA community often have to test their algorithms through field experiments, which are expensive and time consuming. Underwater experiments often involve ships, crews, and specialized equipment and are, therefore, significantly more costly and labor intensive than terrestrial communication systems. Therefore, it is of great interest to find alternative methods to evaluate underwater communication systems with reasonable costs.

Although experimental data collected in most field experiments are often narrowly focused on specific channel coding, bit-to-symbol mapping, and waveform modulation schemes, two field data reuse approaches [8], [9], [10], [11] have emerged in the recent literature that attempt to combine field experiments with computer simulations to evaluate new SUTs. One is the replay-based approach, which involves incorporating the measured channel impulse response (CIR) from real-world experiments into a simulation testbed and comparing different SUTs in a quasi-realistic environment [8], [9]. This approach describes the UWA channel as a time-varying linear convolution process on a fine time scale, but suffers from the loss of the nonlinear and nonstationary properties associated with the actual passband UWA channels. As a result, replay-based simulation tends to predict overly optimistic performance compared to field experimental studies.

Another approach is the data dithering reuse (DDR) method [10], [11], [12], which utilizes the postexperimental data to evaluate different forward error correction (FEC) coding and different bit-to-symbol mapping schemes through a dithering process. The DDR method elegantly adds dithering to coded bits and/or mapped symbols in the original experimental scheme (OES) such that the originally transmitted passband data preserve their experience of the real-world acoustic channel while testing different FEC coding schemes and/or bit-to-symbol mapping schemes of the SUTs. At the receiver, reverse dithering is added to the OES to recover the bits of the SUT, allowing the bit error rate (BER) of different coding strengths and different constellation orders to be tested without the need for additional field experiments. This approach provides significant opportunities for existing experimental data, and the performance of the SUT is shown to preserve the fidelity of field experiments

Manuscript received 18 August 2023; revised 9 February 2024; accepted 11 May 2024. The work of Yukang Xue and Yahong Rosa Zheng was supported in part by the U.S. National Science Foundation Under Award IIP 1853258. *(Corresponding author: Yukang Xue.)*

Associate Editor: C. C. Tsimenidis.

The authors are with the Department of Electrical and Computer Engineering, Lehigh University, Bethlehem, PA 18015 USA (e-mail: yux615@lehigh.edu; chrisqinxz@gmail.com; yrz218@lehigh.edu).

Digital Object Identifier 10.1109/JOE.2024.3412202

1558-1691 © 2024 IEEE. Personal use is permitted, but republication/redistribution requires IEEE permission.
See https://www.ieee.org/publications/rights/index.html for more information.

Authorized licensed use limited to: LEHIGH UNIVERSITY. Downloaded on August 15,2024 at 22:00:01 UTC from IEEE Xplore. Restrictions apply.

This article has been accepted for inclusion in a future issue of this journal. Content is final as presented, with the exception of pagination.

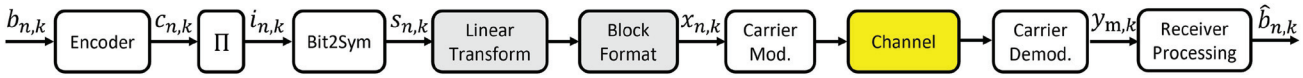

Fig. 1. Signal flow in the unified system model of SCM and OFDM.

and to be more reliable than replay-based or computer-simulated channel models. In addition, a modification to the replay-based simulation technique using residual prediction error (RPE) is presented in [11], which intuitively outperforms the direct replay simulation in terms of channel parameterization and environmental noise modeling.

In this article, we extend the DDR method of [11] for the postexperimental evaluation of SUTs beyond FEC and symbol mapping to waveform modulation schemes and for multiple-input multiple-output (MIMO) [13] systems. The proposed waveform dithering method bridges the gap between single-carrier modulation (SCM) and orthogonal frequency-division multiplexing (OFDM), thus enabling the cross evaluation of SCM and OFDM. Specifically, the proposed waveform DDR method consists of three steps: first, the signal blocks of the OES are modified to form the signal blocks of the SUTs; second, waveform dithering sequences between the OES and the SUT are generated, particularly when the SCM signals have different block lengths and the OFDM signals have cyclic prefix (CP) or zero-padding (ZP) guard intervals; third, the UWA channel is estimated as a time-varying linear system, and reverse dithering sequences are generated and subtracted from the corresponding OES received signal data sets. The reverse-dithered data sets are then ready for evaluating the SUT scheme. We demonstrate the effectiveness of the proposed DDR method and to cross evaluate SCM and OFDM with the OES, DDR, and RPE-enhanced replay methods using the data from undersea 2008 Surface Processes and Acoustic Communications Experiment (SPACE08). All methods use the same channel estimation and the MIMO soft-decision frequency-domain Turbo equalization (FDTE) [14], [15], [16], [17] to detect symbols and generate BER performance. We also define a new similarity index measure (SIM) to characterize the prediction performances. The numerical results confirm that the proposed waveform DDR method predicts BER performance that is closer to that of the OES than the RPE-enhanced replay method. Both the DDR and RPE-enhanced replay methods may predict better or worse performance than the OES evaluation and thus can be used as cost-effective tools for UWA communication research. The proposed waveform DDR method has a smaller SIM, more accurate prediction and robustness, and can be used as a cost-effective tool for UWA communication studies.

II. System Model

First, we introduce a linear transform block and a block format block to the communication system models, as shown in Fig. 1, so that the structure of SCM and OFDM are unified. Note that n, m, and k denote the transmitter, receiver, and time indices, respectively. The $N \times M$ MIMO UWA communication system has N projectors and M hydrophones, and the data block length of the baseband transmitted signal $x_{n,k}$ is K.

At the transmitter, the information bit stream $b_{n,k}$ of the nth projector at instant k is independently encoded (Encoder), interleaved (Π), and mapped (Bit2Sym), where $c_{n,k}$, $i_{n,k}$, and $s_{n,k}$ denote the encoded bit, the interleaved bit, and the mapped symbol, respectively. The mapped baseband symbols $s_{n,k}$ are linearly transformed and formatted into the baseband waveform streams $x_{n,k}$, for $n = 1, \ldots, N$ and $k = 1, \ldots, K$. For the SCM, the linear transform is simply an identity matrix with a size of $K \times K$ for each n. The block formatter takes the K symbols per block and inserts a guard interval if needed. For OFDM, the linear transform is the K-point inverse fast Fourier transform (IFFT) matrix for each n. The block formatter also takes the transformed symbols and inserts the CP or ZP. The baseband waveform signal $x_{n,k}$ is pulse-shaped and modulated onto the carrier frequency.

The received signal is carrier demodulated and is fed into the baseband processing block. The details of the receiver baseband processing are omitted in the figure, which usually includes matched filtering, symbol synchronization, channel estimation, channel equalization, and FEC decoding. The equivalent baseband signal of the mth hydrophone at instant k is expressed as

$$y_{m,k} = g_{n,m}(x_{n,k}) + \mathrm{z}_{m,k} \tag{1}$$

where $g_{n,m}(\cdot)$ is the end-to-end response of the baseband equivalent channel linking the nth projector to the mth hydrophone, and $\mathrm{z}_{m,k}$ is the ambient noise. Note that the UWA channel model $g_{n,m}(\cdot)$ is often nonlinear and/or wide-sense nonstationary, but the commonly used convolution of CIR simplifies the relationship between the channel inputs and outputs into a linear time-varying model as

$$\tilde{y}_{m,k} = \sum_{n=1}^{N} \sum_{l=0}^{L-1} h_{m,n}^{k,l} x_{n,k-l} + z_{m,k} \tag{2}$$

where L is the channel length, and $\{h_{n,m}^{k,l}\}_{l=0}^{L-1}$ is the lth tap of the time-varying channel impulse response (TV-CIR), and $z_{m,k}$ is the zero mean additive white Gaussian noise whose power is assumed to be σ_z^2. Furthermore, the linear CIR is often assumed to be wide-sense stationary with a time-invariant autocorrelation function $R_{hh}(t, t+\tau) = R_{hh}(\tau)$. The two simplified assumptions about UWA channels cause the computer simulation models to produce much better performance over the field experiments, and the data reuse approaches are aimed at reducing the evaluation gap.

In the proposed DDR scheme, it is the reuse of the field data that improve the fidelity to real UWA channels $g_{n,m}(\cdot)$ by avoiding complete reliance on (2) to construct the channel model. Nevertheless, the simplified linear channel model (2) is often used in designing the receiver processing algorithms, such as channel estimation and channel equalization. In this case, we can judiciously split the data block

Authorized licensed use limited to: LEHIGH UNIVERSITY. Downloaded on August 15,2024 at 22:00:01 UTC from IEEE Xplore. Restrictions apply.

This article has been accepted for inclusion in a future issue of this journal. Content is final as presented, with the exception of pagination.

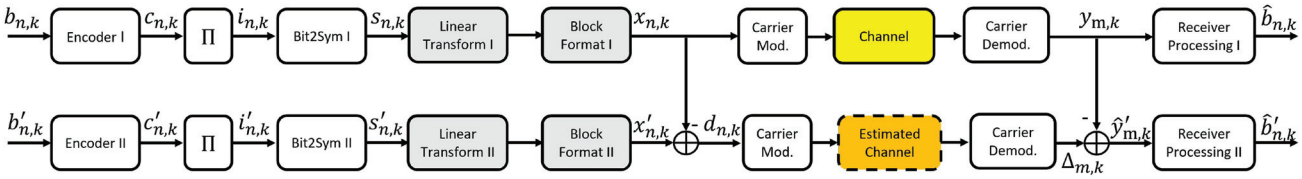

Fig. 2. Signal flow of the DDR method.

to guarantee that the partitioned subblock is shorter than the equivalent channel coherence time. Therefore, the channel becomes linear time invariant in a short time, $h_{m,n}^{k,l} \approx h_{m,n}^{(l)}$. Denote the received symbol block at the mth hydrophone as $\mathbf{y}_m = [y_{m,1}, y_{m,2}, \ldots, y_{m,K}]^T$. Concatenate the receive vectors of all hydrophones as $\mathbf{y} = [\mathbf{y}_1^T, \mathbf{y}_2^T, \ldots, \mathbf{y}_M^T]^T$. The corresponding data block transmitted by the nth projector is denoted as $x_n = [x_{n,1}, x_{n,2}, \ldots, x_{n,K}]^T$. Concatenate transmit vectors of all projectors as $\mathbf{x} = [\mathbf{x}_1^T, \mathbf{x}_2^T, \ldots, \mathbf{x}_N^T]^T$. Then, the simplified baseband MIMO system is modeled as

$$\tilde{\mathbf{y}} = \mathbf{H}\mathbf{x} + \mathbf{z} \tag{3}$$

where the reconstructed baseband received signal $\tilde{\mathbf{y}}$ takes a similar form as $\mathbf{y}$, and the noise vector

$$\mathbf{z}_m = [z_{m,1}, z_{m,2}, \ldots, z_{m,K}]^T$$

and the concatenated $\mathbf{z} = [\mathbf{z}_1^T, \mathbf{z}_2^T, \ldots, \mathbf{z}_M^T]^T$ are assumed to be independent identically distributed (i.i.d) white Gaussian noise. The MIMO channel matrix $\mathbf{H}$ is defined as

$$\mathbf{H} \triangleq \begin{bmatrix} \mathbf{h_{L-1}} & \cdots & \mathbf{h}_0 & \cdots & 0 \\ \vdots & \ddots & \ddots & \ddots & \vdots \\ 0 & \cdots & \mathbf{h}_{L-1} & \cdots & \mathbf{h}_0 \end{bmatrix} \tag{4}$$

with

$$\mathbf{h}_l \triangleq \begin{bmatrix} h_{1,1}^{(l)} & h_{1,2}^{(l)} & \cdots & h_{1,N}^{(l)} \\ \vdots & \vdots & \ddots & \vdots \\ h_{M,1}^{(l)} & h_{M,2}^{(l)} & \cdots & h_{M,N}^{(l)} \end{bmatrix}. \tag{5}$$

Fig. 2 illustrates the signal flow of the proposed waveform DDR method. The top row is the OES data flow, which is the same as that depicted in Fig. 1, and the baseband equivalent channel is $g_{n,m}(\cdot)$. Parallel to the OES data flow, the bottom row is the SUT data flow where the SUT information bit stream $b'_{n,k}$ is encoded (Encoder II), interleaved (Π), and mapped (Bit2Sym II) to $c'_{n,k}$, $i'_{n,k}$, and $s'_{n,k}$, respectively. The channel coding and symbol mapping of SUT and OES can be the same or different. Assuming that OES and SUT use different waveform modulation methods, their linear transforms and block formatters are different, yielding different symbols, $x_{n,k}$ and $x'_{n,k}$, respectively. The difference between the modulated symbols is defined as the dithering sequence, $d_{n,k} \triangleq x_{n,k} - x'_{n,k}$. Then, the dithering signal passes through the estimated linear channel $h_{n,m}^{k,l}$, resulting in the reverse dithering sequence $\Delta_{m,k}$. The received signal of the SUT $y'_{m,k}$ is derived from the received baseband signal of the OES $y_{m,k}$ as $y'_{m,k} = y_{m,k} - \Delta_{m,k}$, where the physical channel effect on the received signal is preserved. Note that the reverse dithering in the waveform DDR may be incorporated with the dithering for FEC and constellation DDR proposed in [11].

Compared to the proposed DDR scheme, the signal flow of the RPE-enhanced replay method [11] is shown in Fig. 3. First, the RPE-enhanced replay method uses the transmitted signal of the OES to estimate the TV-CIR. Then, it uses the estimated channel to construct the predicted signals $\tilde{y}_{m,k}$ and computes the RPE between the actually received and the predicted OES signals at the receiver: $e_{m,k} = y_{m,k} - \tilde{y}_{m,k}$. Next, the RPE-enhanced replay method passes the transmitted signals of the SUT directly through the estimated channel and adds ambient noise of the desired signal-to-noise ratio (SNR), resulting in the channel replay output $\tilde{y}'_{m,k}$. Finally, the RPE $e_{m,k}$ is injected into the channel replay output such that $\hat{y}'_{m,k} = \tilde{y}'_{m,k} + e_{m,k}$, where $\hat{y}'_{m,k}$ is used to evaluate the SUT performance. The vector form of the received signal for the RPE-enhanced replay method is

$$\hat{\mathbf{y}}'_k = \mathbf{H}_{k-1}\mathbf{x}'_k + \mathbf{e}_k + \mathbf{z}_k \tag{6}$$

where $\mathbf{H}_{k-1}$ is the TV-CIR estimated at instant $(k-1)$, $\mathbf{e}_k$ is the vectorized $e_{m,k}$, which is the least-squares residual signal prediction error of the OES, and $\mathbf{z}_k$ is the noise vector. Adding RPE to the channel replay output accounts for channel estimation errors and achieves more accurate performance predictions than the conventional direct replay simulator.

Comparing Figs. 2 and 3, both the proposed waveform DDR method and the RPE-enhanced replay method utilize the existing OES data to maintain the effect of channel nonlinearity experienced by the received signal and compensate for the channel dynamics. The difference is that the RPE-enhanced replay method uses RPE to characterize the difference between the actual UWA channel and the estimated channel and injects it into the SUT, while the proposed DDR method directly retains the actual channel characteristics that may be missed by the linear TV-CIR estimated often with the wide-sense stationary assumptions.

III. Block Preparation for DDR

It is commonly known that the block structures of the OFDM and the SCM signals are quite different because the OFDM blocks require CP or ZP insertion, while the SCM may be transmitted in continuous blocks. To cross evaluate these two modulation waveforms, the SCM and OFDM data blocks must be converted before dithering. In general, the block lengths in OFDM and SCM are specific to their own applications and system designs, so the block lengths of OES data and SUT data are usually different. To match the block sizes for cross evaluation, the OES-SCM transmitted data blocks are partitioned

Authorized licensed use limited to: LEHIGH UNIVERSITY. Downloaded on August 15,2024 at 22:00:01 UTC from IEEE Xplore. Restrictions apply.

This article has been accepted for inclusion in a future issue of this journal. Content is final as presented, with the exception of pagination.

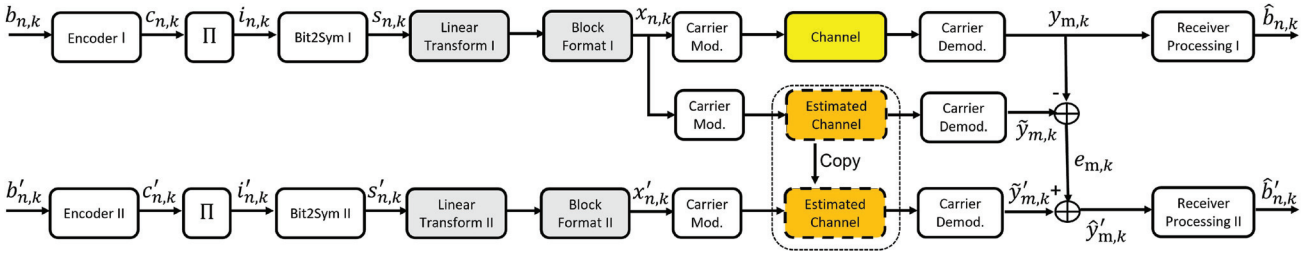

Fig. 3. Signal flow of the RPE-enhanced direct replay method.

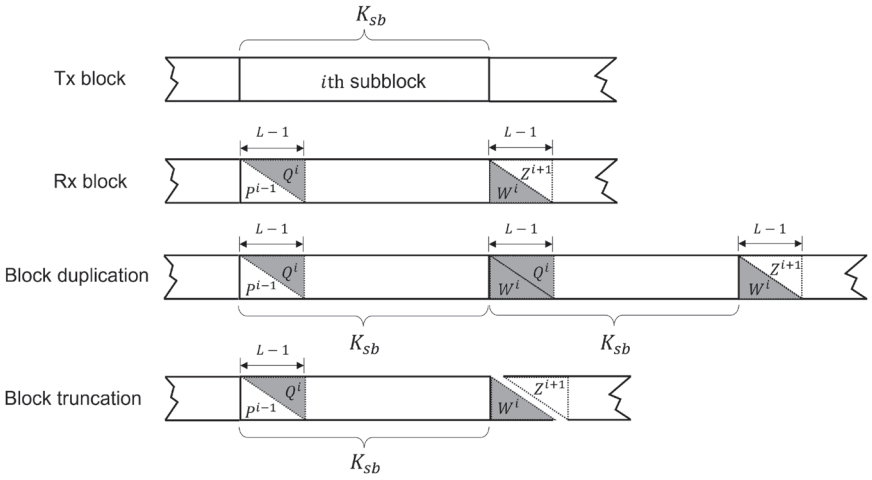

Fig. 4. Block preparation before waveform dithering.

into subblocks of size K_{sb} to ensure that $K_{sb} = K_{\text{OFDM}}$, where K_{OFDM} is the block length of the SUT-OFDM. The received signals corresponding to the CP or ZP are reconstructed and added to the block. Similarly, several OFDM transmitted data blocks may be concatenated to form an extended data block of size K_{cb} satisfying $K_{cb} = K_{\text{SCM}}$, where K_{SCM} is the SUT-SCM block length. However, direct partition or concatenation of the received signal blocks induces interblock interference (IBI) due to the frequency-selective channels. Therefore, interference cancellation techniques are required in block preparation of the received signals, which will be detailed in Section III-A. The OFDM CP/ZP insertion and the corresponding received signal reconstruction are detailed in Section III-B.

A. Block Duplication and Truncation

As shown in Fig. 4, block duplication is the process of combining multiple subblocks of the OES to form a longer block for the SUT. In contrast, block truncation refers to extracting a subblock from the middle of a long block and discarding the tail of the long block. Both techniques may be needed when preparing an OES-OFDM for evaluating an SUT-SCM and vice versa.

Considering the ith subblock of the transmitted signal in Fig. 4, the $(i-1)$th subblock passes through the frequency-selective channel of length L and results in the precursor interference $P_{m,k}^{i-1}$. Similarly, the ith subblock causes postcursor interference $W_{m,k}^{i}$ to the $(i+1)$th subblock. The length of precursor and postcursor interference is $L-1$, which means that the first $L-1$ and last $L-1$ symbols of each received subblock signal have to be modified. The precursor interference from the $(i-1)$th subblock to the ith subblock is reconstructed as

$$P_{m,k}^{i-1} = \sum_{n=1}^{N} \sum_{l=k+1}^{L-1} \hat{h}_{m,n}^{i-1}(l) x_{n,K_{sb}-l+k}^{i-1} \tag{7}$$

where $x_{n,K_{sb}-l+k}^{i-1}$ is the $(K_{sb}-l+k)$th symbol of the $(i-1)$th subblock

$$\mathbf{x}_n^{i-1} = [x_{n,0}^{i-1}, x_{n,1}^{i-1}, \ldots, x_{n,k_{sb}-1}^{i-1}]^T \tag{8}$$

and $\hat{h}_{m,n}^{i-1}(l)$ is the lth estimated channel tap corresponding to the (n,m)th channel link. By removing the precursor interference $P_{m,k}^{i-1}$ from the current subblock $y_{m,k}^{i}$, we get

$$Q_{m,k}^{i} = y_{m,k}^{i} - P_{m,k}^{i-1}, \quad \text{for } 0 \le k \le L-2 \tag{9}$$

where $Q_{m,k}^{i}$ is the first $L-1$ symbols of the ith received subblock.

Similarly, the reconstructed postcursor interference $W_{m,k}^{i}$ from the i th subblock to the $(i+1)$ subblock is given

$$Z_{m,k}^{i+1} = \sum_{n=1}^{N} \sum_{l=0}^{k} \hat{h}_{m,n}^{i+1}(l) x_{n,k-l}^{i+1} \tag{10}$$

$$W_{m,k}^{i} = y_{m,k}^{i+1} - Z_{m,k}^{i+1}, \quad \text{for } 0 \le k \le L-2 \tag{11}$$

Authorized licensed use limited to: LEHIGH UNIVERSITY. Downloaded on August 15,2024 at 22:00:01 UTC from IEEE Xplore. Restrictions apply.

This article has been accepted for inclusion in a future issue of this journal. Content is final as presented, with the exception of pagination.

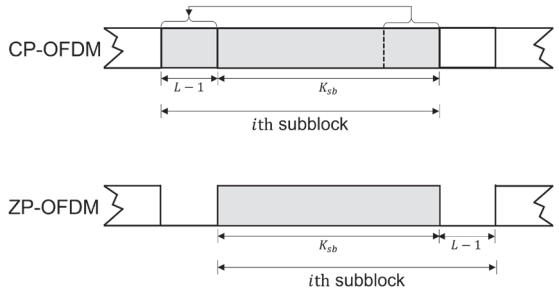

Fig. 5. Transmitted signal for CP-OFDM and ZP-OFDM.

where $Z_{m,k}^{i+1}$ is the first $L-1$ symbols of the $(i+1)$th subblock $y_{m,k}^{i+1}$. Note that (7) and (10) use the linear channel model of (2) to compute the interference, so that the nonlinear effects of the OES channel are preserved in (9) and (11) for $Q_{m,k}^{i}$ and $W_{m,k}^{i}$, respectively.

After computing $P_{m,k}^{i-1}$, $Q_{m,k}^{i}$, $Z_{m,k}^{i+1}$, and $W_{m,k}^{i}$, the received data blocks may be truncated, extracted, duplicated, or concatenated. To truncate at the end of the ith subblock, the received signals after the end of the ith subblock are to be removed and the $(L-1)$ sequences of $W_{m,k}^{i}$ are appended. To extract the ith subblock from a long transmit block, the corresponding received signals at the first $(L-1)$ symbol periods are replaced by $Q_{m,k}^{i}$, and the end of the subblock is appended with $W_{m,k}^{i}$. To duplicate a subblock i and insert it between the ith and $(i+1)$th subblocks, the first $(L-1)$ symbol periods of the inserted subblock in the received signal have to be replaced by $Q_{m,k}^{i}+W_{m,k}^{i}$, as shown in Fig. 4. If the ith and $(i+1)$th subblocks are separated by a gap in the OES and the SUT would concatenate the two subblocks, then the received signals corresponding to the two subblocks may be joined together by adding the tail of the ith subblock to the first $(L-1)$ symbol periods of the $(i+1)$th subblock, i.e., $W_{m,k}^{i}+y_{m,k}^{i+1}$ for $k=0,\ldots,L-2$.

B. OFDM CP/ZP Insertion

OFDM schemes use CP/ZP to facilitate circular convolution and eliminate IBI, while SCM schemes normally use long data blocks without gaps. Therefore, cross evaluation between SCM and OFDM has to bridge the differences in transmit data formats and their effects on the received signals. To convert the OES-OFDM blocks to the SUT-SCM blocks, the OFDM subblocks may be simply concatenated using the techniques in Section III-A to form the received signals of SCM blocks. On the other hand, it is much involved to convert a data block from OES SCM to SUT-OFDM. First, the transmit SCM data block is split into subblocks of length K_{sb}, which is the length of the OFDM data blocks. Assume that a CP/ZP of length $L-1$ is inserted in between every two OFDM blocks. As shown in Fig. 5, if a CP is inserted, the last $(L-1)$ symbols of the ith subblock are copied and added at the beginning of the subblock. If a ZP is desired, simply insert $(L-1)$ symbol periods of the gap between the two subblocks. Both methods are used to solve the problem of intersymbol interference, which is caused by the multipath effects of the wireless channel. CP reduces the spectral efficiency of the OFDM system because it increases the symbol duration without increasing the data payload, while ZP increases receiver complexity and introduces slightly more nonlinear distortion when implemented.

The following describes how to convert OES-SCM blocks into SUT CP-OFDM and ZP-OFDM, respectively. When SUT-OFDM uses ZP, two steps are required to construct the corresponding received signals: 1) reconstruct and remove the precursor and postcursor interference induced by the $(i-1)$th and $(i+1)$th subblocks; and 2) extract the tail of the current subblock and overlap-add (OLA) the tail to the beginning of the subblock. Fig. 6 shows transmit data blocks of SCM and the corresponding received signals, where the precursor and postcursor interferences of $P_{m,k}^{i-1}$, $Q_{m,k}^{i}$, $Z_{m,k}^{i+1}$, and $W_{m,k}^{i}$ are calculated by (7), (9), (10), and (11), respectively. After removing the precursor interference $P_{m,k}^{i-1}$ and postcursor interference $Z_{m,k}^{i+1}$, the response of the last $L-1$ symbols of the ith subblock $W_{m,k}^{i}$ is overlap-added on $Q_{m,k}^{i}$ such that

$$y_{m,k}^{i} := W_{m,k}^{i}+Q_{m,k}^{i}, \quad \text{for } 0\le k\le L-2. \tag{12}$$

The remaining $K_{sb}-L+1$ symbol periods of $y_{m,k}^{i}$ remain unchanged. This corresponds to the processed ith subblock of the ZP-OFDM received signals, which is ready to be transformed into the frequency domain and dithered. When SUT OFDM is CP-inserted, the last $(L-1)$ symbols of the received symbols are copied and appended to the beginning of the ith subblock, resulting in a subblock of length $K_{sb}+L-1$, as shown in Fig. 7. This can be achieved through the following three steps: 1) copy and append the last $(L-1)$ symbols to form the CP; 2) reconstruct and remove the precursor and postcursor interference induced by the $(i-1)$th and $(i+1)$th subblocks; and 3) extract the tail of the current subblock and OLA it to the beginning of the subblock. Note that since the CP is discarded in the subsequent processing, we only consider the K_{sb} part for simplicity. Therefore, we remove the precursor interference $P_{m,k}^{i-1}$ and add the response of the last $L-1$ symbols of the ith subblock $W_{m,k}^{i}$ to get the SUT OFDM received signals ready for the fast Fourier transform (FFT). When only considering the K_{sb} part of the received signals, the calculation formula has the same form as (12).

In both CP and ZP OFDM conversions, we use OLA to convert OES-SCM signals for consistency. If the transmitted OES-SCM data blocks contain gaps, these can be treated as zero symbols when computing the IBI, and their effects can be removed from the received signals easily.

IV. Cross Evaluation of SCM and OFDM Schemes

When the data blocks of the OES signals are prepared to match the desired SUT block structures, the next step in the DDR cross-evaluation process is to compute the dithering and reverse dithering signals. As mentioned in Section II, the received signal of the SUT, denoted as $\hat{y}'_{m,k}$, is generated using the reverse dithering signals $\Delta m,k$ and the received OES signal $y_{m,k}$. In this work, we use the MIMO soft-decision FDTE technique [14], [16] at the receiver end. The motivation for choosing FDTE

Authorized licensed use limited to: LEHIGH UNIVERSITY. Downloaded on August 15,2024 at 22:00:01 UTC from IEEE Xplore. Restrictions apply.

This article has been accepted for inclusion in a future issue of this journal. Content is final as presented, with the exception of pagination.

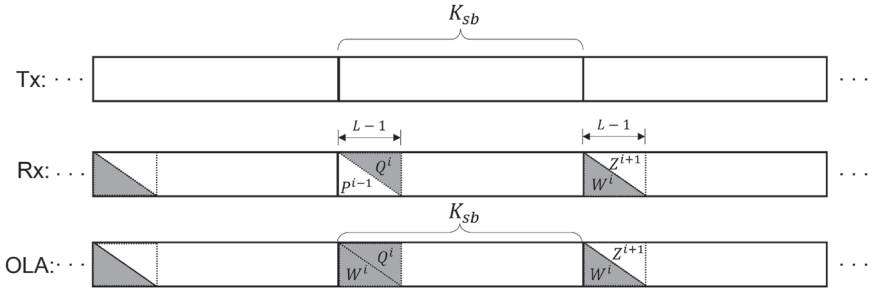

Fig. 6. ZP-OFDM construction from SCM without gaps.

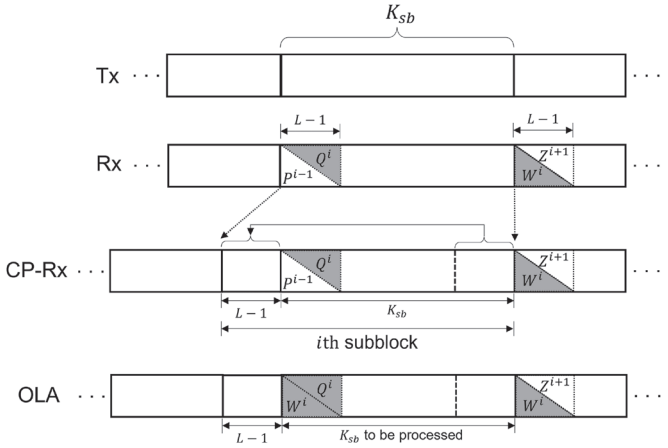

Fig. 7. CP-OFDM construction from SCM without gaps.

is that the OLA operation performed in the block preparation phase has already transformed the equivalent channel into a circular form, enabling the use of frequency-domain equalization to reduce computational complexity. Turbo also enhances the equalizer's ability to combat nonlinear features, improving the accuracy of the evaluation.

The linear time-varying channel model, described by (2), groups the modulated symbols into subblocks of length $K = K_{sb}$. At the receiver, K-point FFT/IFFT is applied to the received signal. After the OLA operation, the linear convolution of the transmitted signal with the TV-CIR is converted into a circular convolution. Therefore, the MIMO system in the proposed framework can be modeled as follows:

$$\tilde{\mathbf{y}} = \hat{\mathbf{H}}\mathbf{x} + \mathbf{z} \tag{13}$$

where $\hat{\mathbf{H}}$ is a block circulant matrix with its first column being $[\mathbf{h}_0^T, \ldots, \mathbf{h}_{L-1}^T, \mathbf{0}_{N\times M(K-L)}]^T$. The noise vector $z_{m,k} = [z_{m,1}, z_{m,2}, \ldots, z_{m,K}]^T$, for $m \in \{1, \ldots, M\}$, and $\mathbf{z} = [z_{1,k}^T, z_{2,k}^T, \ldots, z_{M,k}^T]^T$ may be colored by the OLA operation when no perfect channel state information is available a priori. However, we still treat the noise in (13) as i.i.d white Gaussian to simplify the mathematical derivation.

Let $\mathbf{F}$ be the normalized FFT matrix of size $K \times K$ such that $\mathbf{F}\mathbf{F}^H = \mathbf{I}_K$, where $\mathbf{I}_K$ is the identity matrix of size K and $\mathbf{F}^H$ is the IFFT matrix. Denote the block FFT matrix as $\mathbf{F_M} = \mathbf{I}_M \bigotimes \mathbf{F}$, where $\bigotimes$ represents the Kronecker product of matrices. Multiplying $\mathbf{F}_M$ on both sides of (13), the blockwise time-domain model is converted into the frequency-domain representation

$$\tilde{\mathbf{Y}} = \mathbf{F}_M\tilde{\mathbf{y}} = \mathbf{F}_M\hat{\mathbf{H}}\mathbf{F}_N^H\mathbf{F}_N\mathbf{x} + \mathbf{F}_M\mathbf{z} = \mathbf{T}\mathbf{X} + \mathbf{Z} \tag{14}$$

where $\mathbf{T} = \mathbf{F}_M\hat{\mathbf{H}}\mathbf{F}_N^H$ is the frequency-domain channel matrix and $\mathbf{X} \triangleq \mathbf{F}_N\mathbf{x}$ is the block FFT of the transmit vector. Since $\hat{\mathbf{H}}$ is a block circulant matrix in the time domain, its frequency-domain representation $\mathbf{T}$ is a block diagonal matrix, with $\mathbf{T}_k \in \mathcal{C}^{M\times N}$ being the block diagonal elements defined as

$$\mathbf{T}_k = \begin{bmatrix} \hat{T}_{1,1}^k & \hat{T}_{1,2}^k & \cdots & \hat{T}_{1,N}^k \\ \vdots & \vdots & \ddots & \vdots \\ \hat{T}_{M,1}^k & \hat{T}_{M,2}^k & \cdots & \hat{T}_{M,N}^k \end{bmatrix} \tag{15}$$

where $\hat{T}_{n,m}^k$ is the channel frequency response of the (n,m)th channel link at the kth subcarrier.

We are now ready to derive the relationship between $d_{n,k}$ and $\Delta_{m,k}$ for cross evaluation. In Fig. 2, if the OES uses OFDM and the SUT uses SCM, then Linear Transform I is an IFFT matrix and $x_n = \mathbf{F}_N^H s_n$. Linear Transform II is an identity matrix and $x'_{n,k} = s'_{n,k}$. If the OES uses SCM and the SUT uses OFDM, Linear Transform I is an identity matrix and Linear Transform II is an IFFT matrix. This means $x'_n = \mathbf{F}_N^H s'_n$. In both the cases, the dithering sequence $d_{n,k} = x_{n,k} - x'_{n,k}$. Since the physical nonlinear channels $g(\cdot)$ is inaccessible, the reverse dithering sequence $\Delta_{m,k}$ may be computed by the linear channel model (13) as $\mathbf{\Delta} = \hat{\mathbf{H}}(\mathbf{x} - \mathbf{x}') = \hat{\mathbf{H}}\mathbf{d}$.

Applying the reverse dithering operation to the prepared OES signals results in the SUT-received signals

$$\mathbf{y}' = \mathbf{y} - \mathbf{\Delta} = \mathbf{g}(\mathbf{x}' + \mathbf{d}) + \mathbf{z} - \mathbf{\Delta}. \tag{16}$$

Comparing (16) with the linear model output $\tilde{\mathbf{y}}' = \hat{\mathbf{H}}\mathbf{x}' + \mathbf{z}$, it is clear that the proposed dithering method (16) preserves the nonlinear channel response in the SUT received signals.

After obtaining the received signal blocks for both the OES and the SUT, frequency-domain decision-feedback Turbo equalization is applied to both the SCM and the OFDM signals for fair comparison. The FDTE first processes the signals $\mathbf{Y}$ in the frequency domain and then utilizes the feedback information $\breve{\mathbf{x}}^{(j-1)}$ from the $(j-1)$th Turbo iteration to improve the detection performance [14]

$$\hat{\mathbf{x}}^{(j)} = \mathbf{F}_N^H\mathbf{W}\mathbf{Y} - \mathbf{F}_N^H\mathbf{D}\mathbf{F}_N\breve{\mathbf{x}}^{(j-1)} \tag{17}$$

Authorized licensed use limited to: LEHIGH UNIVERSITY. Downloaded on August 15,2024 at 22:00:01 UTC from IEEE Xplore. Restrictions apply.

This article has been accepted for inclusion in a future issue of this journal. Content is final as presented, with the exception of pagination.

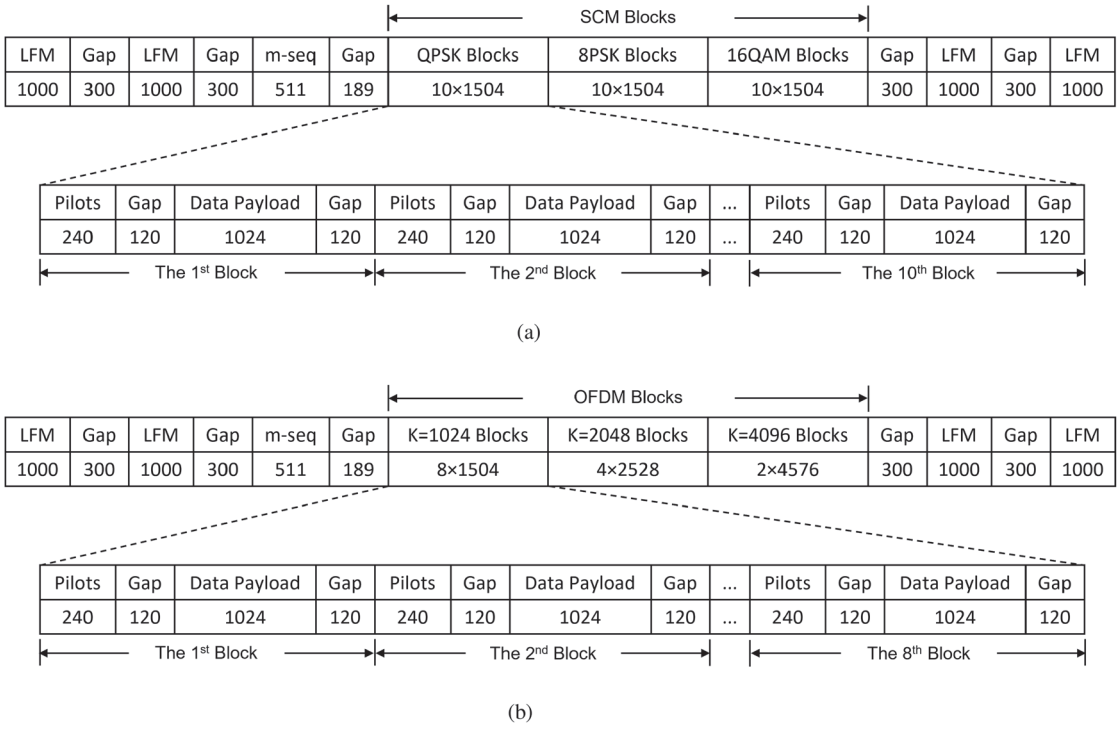

Fig. 8. Selected data structure of (a) SCM and (b) OFDM schemes in the SPACE08.

where $\mathbf{W} = \text{Bdiag}\{\mathbf{W}_k\}_{k=1}^K$ and $\mathbf{D} = \text{Bdiag}\{\mathbf{D}_k\}_{k=1}^K$ are the frequency-domain feedforward and feedback equalizer matrices, respectively. The soft decision vector in the $(j-1)$th Turbo iteration is

$$\breve{\mathbf{x}}^{(j-1)} = [(\breve{\mathbf{x}}_1^{(j-1)})^T, (\breve{\mathbf{x}}_2^{(j-1)})^T, \ldots, (\breve{\mathbf{x}}_K^{(j-1)})^T]^T$$

and $\breve{\mathbf{x}}_k^{(j-1)} = [\breve{x}_{1,k}^{(j-1)}, \breve{x}_{2,k}^{(j-1)}, \ldots, \breve{x}_{N,k}^{(j-1)}]^T$, with $\breve{x}_{n,k}^{(j-1)}$ being the soft-decision symbol in the $(j-1)$th Turbo iteration. Therefore, the time-domain feedback matrix $\mathbf{F}_N^H \mathbf{D} \mathbf{F}_N$ is a circulant matrix whose diagonal matrix should be set to zero to avoid self-subtraction of the desired estimate at instant k. Consequently, $\mathbf{D}_k$ is a block diagonal matrix whose main diagonal elements follow the constraint

$$\sum_{k=1}^{K} \mathbf{D}_k^H[n,n] = 0. \tag{18}$$

The equalizer coefficients $\mathbf{W}$ and $\mathbf{D}$ are computed by minimizing the mean square error of the equalized symbols in the jth Turbo iteration [18], [19] as

$$\min_{\mathbf{W},\mathbf{D},\lambda_n} \left\{ \mathbf{E}\left\{ (\hat{\mathbf{x}}^{(i)} - \mathbf{x})^H (\hat{\mathbf{x}}^{(i)} - \mathbf{x}) \right\} + \sum_{n=1}^{N} \lambda_n \left(\sum_{k=1}^{K} \mathbf{D}_k^H[n,n] \right) \right\} \tag{19}$$

where λ_n are the Lagrange multipliers.

V. Experimental Results

The proposed cross-evaluation approach was evaluated using postexperimental data collected in the SPACE08. This experiment was conducted by the Woods Hole Oceanographic Institution at the Air-Sea Interaction Tower, located two miles south of the coast of Martha's Vineyard, MA, USA, at a sea depth of approximately 15 m in October 2008. The OFDM and SCM signals were transmitted and received at distances of 200 and 1000 m. The transmit equipment consisted of four transducers numbered 0–3. Transducer 0 was mounted on a stationary tripod about 4 m above the sea bottom, and transducers 1–3 were evenly mounted on a vertical array with an intertransducer spacing of 50 cm. The top transducer in the array was about 3 m above the sea bottom. The average wave height and wind speed were 1.25 m and 5.395 m/s, respectively. The carrier frequency was $f_c = 13$ kHz and the symbol interval was $T_s = 0.1024$ ms. The transmit filter was a root-raised cosine filter with a rolloff factor of 0.2, and the occupied channel bandwidth was 11.7188 kHz. The transmission frame structure is depicted in Fig. 8. SCM blocks were transmitted in the first-minute packet, and OFDM blocks were transmitted in the second-minute packet. The frame began with linear frequency modulation (LFM) signals and an m-sequence, followed by three SCM/OFDM packets, and ended with a trailing LFM signal. The SCM and OFDM blocks had a similar subblock structure, with subblock sizes of 1024, 2048, and 4096. An analysis of the channel scattering function with the m-sequence revealed that the maximum Doppler spread of the channel was around 5 Hz. Most of the channel energy was concentrated within 10 ms, corresponding to a channel with an approximate length of 100 taps. We focused on the 2×12

Authorized licensed use limited to: LEHIGH UNIVERSITY. Downloaded on August 15,2024 at 22:00:01 UTC from IEEE Xplore. Restrictions apply.

This article has been accepted for inclusion in a future issue of this journal. Content is final as presented, with the exception of pagination.

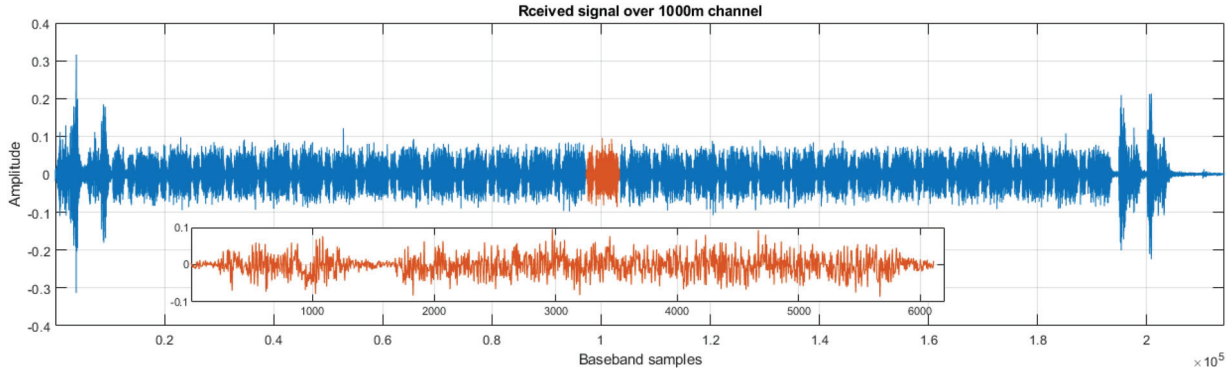

Fig. 9. Example of the received signals in a 1000-m channel.

MIMO scheme, where 30 files of 200-m transmission (S3, S4) and 25 files of 1000-m transmission (S5, S6) were processed for the OES SCM scheme; 19 files of 200-m transmission and 15 files of 1000-m transmission were processed for the OES OFDM scheme. Fig. 9 demonstrates an example of a received OFDM signal in 1000-m transmission, where one subblock is expanded in the subplot. Both the OFDM and the SCM schemes used a rate-1/2 convolutional channel encoder with the generator polynomial $[G_1, G_2] = [17, 13]_{\text{oct}}$. Bit-to-symbol mapping used quadrature phase-shift keying (QPSK) or 16-ary quadrature amplitude modulation (16QAM) in both SCM and OFDM schemes. Many details of the experiment are available in [20], [21], and [22] and are omitted here for the sake of brevity.

In this work, we used several pairs of SCM and OFDM experimental data sets with subblock lengths (1024, 2048, 4096) and bit-to-symbol mappings (QPSK, 16QAM) to compare the cross-evaluation methods DDR and RPE-enhanced channel replay. The OFDM transmission used zero padding in this experiment. We used OES-SCM and OES-OFDM to denote the original experimental data sets, while DDR-SCM and RPE-SCM denote the generated SCM data sets from the original OFDM experiments, and DDR-OFDM and RPE-OFDM denote the generated OFDM data sets from the original SCM experiments. The six data sets were processed with the same FDTE equalizer using parameters $L = 120$, $K_1 = 120$, and $K_2 = 60$. The FDTE coefficients were updated at each iteration per data subblock rather than per data symbol. The maximum number of Turbo iterations was set to 2. The CIRs were obtained by the same channel estimation algorithm using the transmitted and received subblock data in the OES data sets. The channel estimates were updated once per subblock. The RPE-enhanced replay simulation was modified from [11].

The BER distributions of the OES, DDR, and RPE data sets are compared in Figs. 10 and 11 using all the data sets of the transmission scenarios. For QPSK modulation with 200-m transmissions, the BER distributions of the DDR-OFDM and DDR-SCM were between the performance of OES-OFDM and OES-SCM for all block sizes, as shown in Fig. 10(a)–(c). On the contrary, the performance of the RPE method was greatly affected by the different block sizes. When the block size was 1024 or 2048, as shown in Fig. 10(a) and (b), the BER distributions of the RPE data sets also fell between the two OES data sets. When the block size was 4096, as shown in Fig. 10(c), the BER of the RPE data sets deteriorated significantly and the performance was much worse than the two OES data sets. In QPSK 1000-m transmissions, the BER distributions of the DDR-OFDM data sets were between the two OES data sets for all three block sizes, as shown in Fig. 10(d)–(f), while the BER of the DDR-SCM data sets is slightly better than that of the two OES data sets. The RPE data sets were also affected by the different block sizes. When the block sizes were 1024 and 2048, as shown in Fig. 10(d) and (e), the RPE-OFDM achieved slightly worse BER than the two OES data sets, while RPE-SCM achieved slightly better BER than the two OES data sets. When the block size was 4096, as shown in Fig. 10(f), the RPE data sets suffered from huge BER degradation and performed much worse than the two OES data sets.

For 16QAM with all different block sizes, the BER distributions of the DDR-SCM and DDR-OFDM data sets fell between the performance of the OES-OFDM and OES-SCM for both 1000- and 200-m transmissions, as shown in Fig. 11(a)–(f), while more than half of the RPE data sets appeared to be better or worse than the two OES data sets. For example, with a block size of $K = 1024$, the RPE-OFDM with 200-m range and RPE-SCM with 1000-m range achieved better BER than both OES data sets, as shown in Fig. 11(a) and (d), respectively, while the BER of RPE-OFDM with 1000-m range was inferior to the two OES data sets. When the block size was $K = 2048$, RPE-OFDM with 200-m range achieved better BER than both OES data sets, as shown in Fig. 11(b) and RPE-OFDM with 1000-m range had worse BER than both OES data sets, as shown in Fig. 11(e). With a block size of $K = 4096$, all RPE data sets failed to achieve reasonable BERs close to the two OES data sets, as shown in Fig. 11(c) and (f).

Table I shows the average BER of the OES, DDR, and RPE data sets for all experimental scenarios, which exhibit similar trends as the BER distribution plots. In QPSK 200-m transmission, the average BERs of DDR-OFDM and DDR-SCM were mostly in between those of OES-OFDM and OES-SCM for all three block sizes. In contrast, the RPE data sets with a block length of 4096 had a much worse average BER than the OES data sets; the RPE data sets with a block length of 1024 or 2048 had an

Authorized licensed use limited to: LEHIGH UNIVERSITY. Downloaded on August 15,2024 at 22:00:01 UTC from IEEE Xplore. Restrictions apply.

This article has been accepted for inclusion in a future issue of this journal. Content is final as presented, with the exception of pagination.

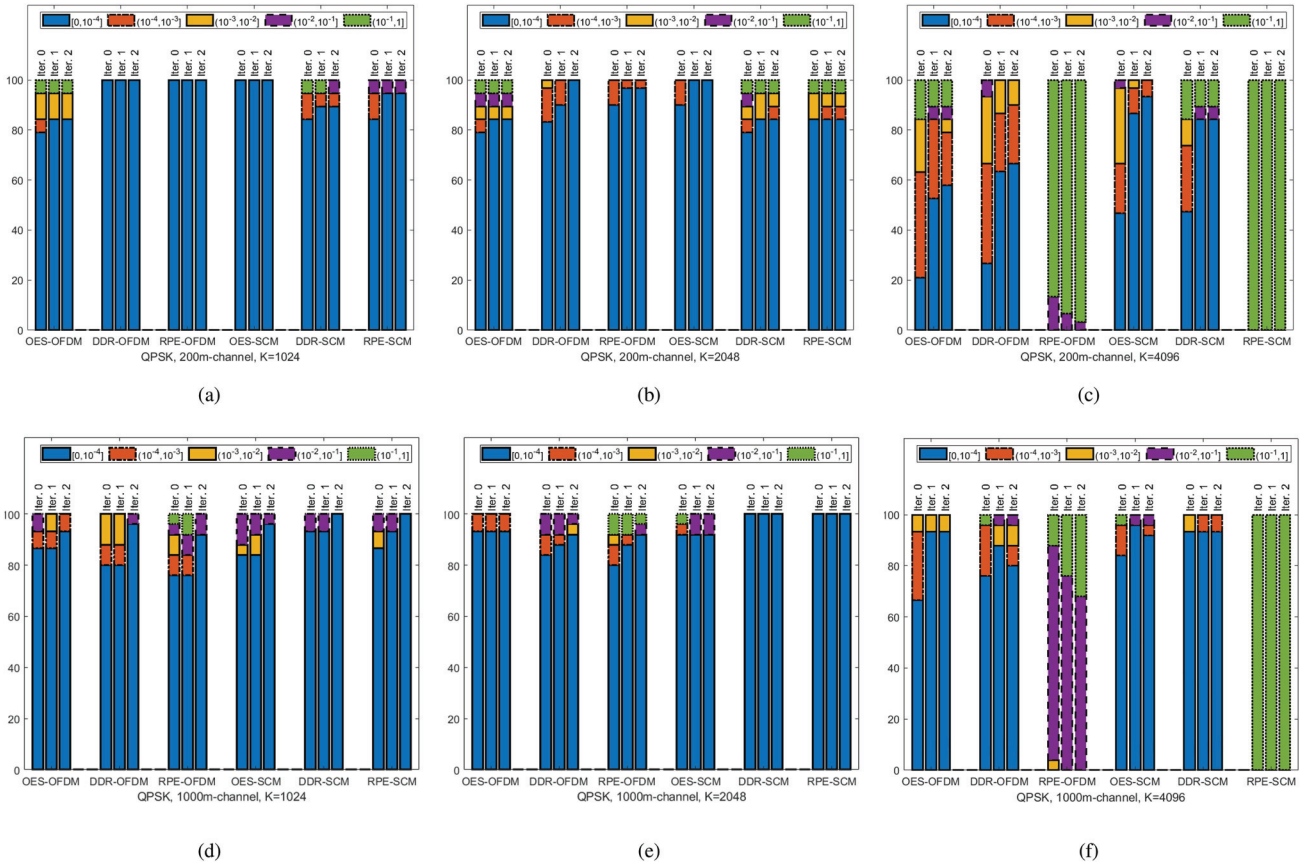

Fig. 10. (a)–(f) BER distributions of OES, DDR, and RPE methods for QPSK modulation.

TABLE I
AVERAGE BER OF OES, DDR, AND RPE METHODS FOR QPSK MODULATION/16QAM

Experimental scenario	OES-OFDM	DDR-OFDM	RPE-OFDM	OES-SCM	DDR-SCM	RPE-SCM
QPSK, K = 1024, 200 m	8.56e-3	0	0	0	5.60e-3	2.17e-3
QPSK, K = 2048, 200 m	2.17e-2	4.48e-5	2.65e-5	1.56e-5	2.20e-2	1.86e-2
QPSK, K = 4096, 200 m	3.41e-2	8.76e-4	1.98e-1	6.18e-4	3.38e-2	3.78e-1
QPSK, K = 1024, 1000 m	4.87e-4	8.67e-4	7.72e-3	3.27e-3	1.02e-3	1.07e-3
QPSK, K = 2048, 1000 m	2.71e-5	2.35e-3	1.14e-2	5.00e-3	0	0
QPSK, K = 4096, 1000 m	1.86e-4	2.80e-3	7.56e-2	4.11e-3	3.26e-5	3.22e-1
16QAM, K = 1024, 200 m	3.54e-2	2.16e-4	5.94e-5	2.08e-4	3.56e-2	2.80e-2
16QAM, K = 2048, 200 m	6.42e-2	1.13e-2	6.94e-3	1.07e-2	6.60e-2	5.69e-2
16QAM, K = 4096, 200 m	1.49e-1	1.06e-1	3.90e-1	1.19e-1	1.54e-1	4.58e-1
16QAM, K = 1024, 1000 m	6.92e-4	1.07e-2	1.64e-2	1.26e-2	2.57e-4	1.70e-4
16QAM, K = 2048, 1000 m	1.29e-3	1.63e-2	2.59e-2	1.74e-2	7.23e-4	1.16e-3
16QAM, K = 4096, 1000 m	2.74e-2	4.36e-2	3.23e-1	4.96e-2	2.58e-2	4.36e-1

Authorized licensed use limited to: LEHIGH UNIVERSITY. Downloaded on August 15,2024 at 22:00:01 UTC from IEEE Xplore. Restrictions apply.

This article has been accepted for inclusion in a future issue of this journal. Content is final as presented, with the exception of pagination.

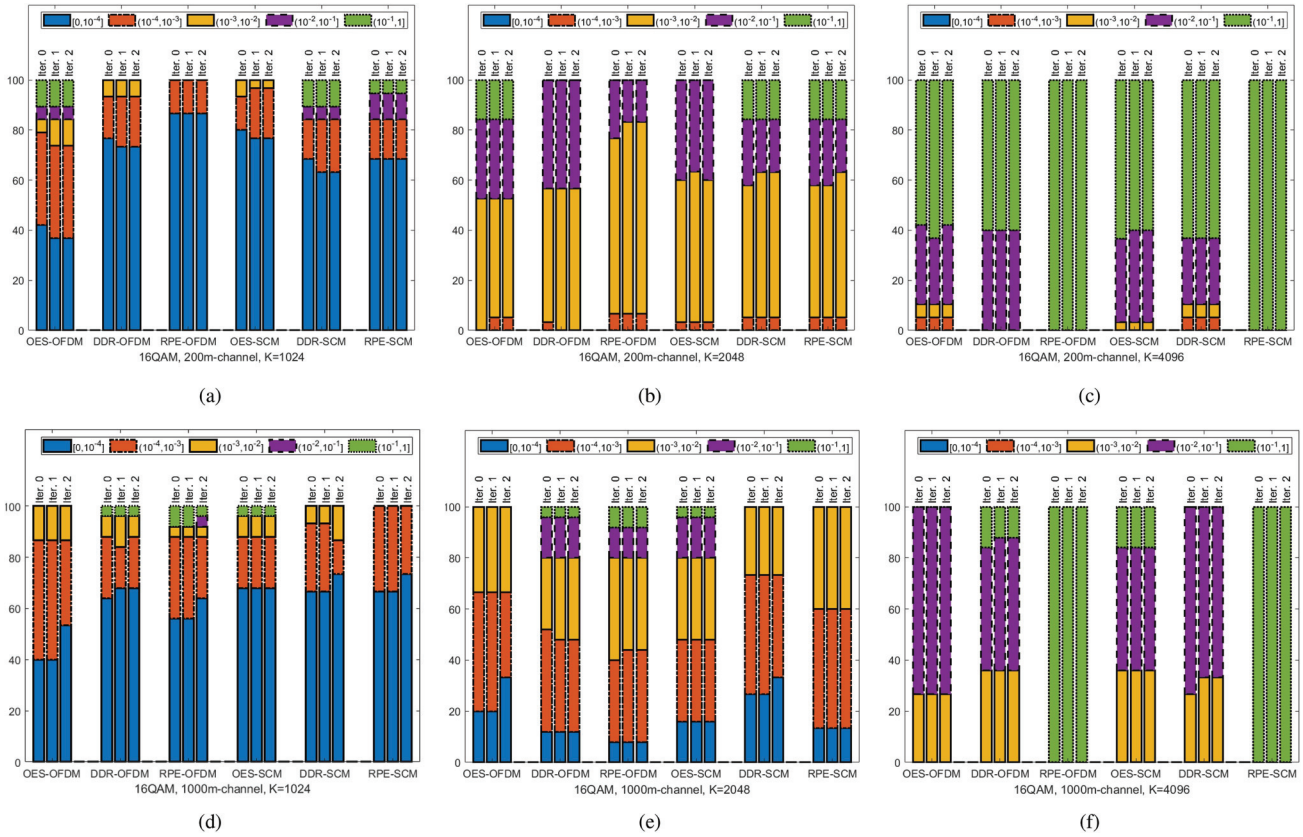

Fig. 11. (a)–(f) BER distributions of OES, DDR, and RPE methods for 16QAM.

average BER between the two OES data sets. In QPSK 1000-m transmissions, the average BER of DDR-OFDM fell between the two OES data sets, while the average BER of DDR-SCM was better than two OES data sets. When the block size was 1024, the average BERs of the RPE data sets were between two OES data sets. When the block length was 2048, the average BER of the RPE-SCM data sets was better than those of two OES data sets, while the average BER of RPE-OFDM data sets was inferior to that of the two OES data sets. When the block length was 4096, the average BERs of the PRE data sets were much worse than the two OES data sets. For 16QAM with all different block sizes, the average BERs of the DDR data sets were almost always between the two OES data sets or very close to one of them, while the average BERs of the RPE data sets were always either too good or too bad compared to the two OES data sets.

We define a new SIM to characterize the prediction performance of the DDR and RPE methods

$$\begin{aligned}&\mathrm{SIM(X,Y)}\\&=\frac{1}{N}\sum_{n=1}^{N}\frac{(\bar{\mu}_{\mathrm{OES,Y}}-\mu_{\mathrm{X,Y},n})^2+(\mu_{\mathrm{OES},\bar{\mathrm{Y}},n}-\mu_{\mathrm{X,Y},n})^2+\epsilon}{(\bar{\mu}_{\mathrm{OES,Y}}-\mu_{\mathrm{OES},\bar{\mathrm{Y}},n})^2+\epsilon}\end{aligned}\tag{20}$$

where SIM() is the SIM for one of the DDR-SCM, DDR-OFDM, RPE-SCM and RPE-OFDM data sets. Let X and Y denote the names of the data sets, where $\mathrm{X}\in\{\mathrm{DDR},\mathrm{RPE}\}$, $\mathrm{Y}\in\{\mathrm{SCM},\mathrm{OFDM}\}$, and $\bar{\mathrm{Y}}\in\{\mathrm{OFDM},\mathrm{SCM}\}$ according to Y. Note that N is the total number of transmission blocks collected in the data sets (X,Y), $\mu_{\mathrm{X,Y},n}$ is the BER of the nth block of the data sets (X,Y), $\mu_{\mathrm{OES},\bar{\mathrm{Y}},n}$ is the BER of the nth block of the OES data sets OES-$\bar{\mathrm{Y}}$, and $\bar{\mu}_{\mathrm{OES,Y}}$ is the average BER of the data sets OES-Y. The regularization parameter ϵ is a very small number to avoid division by zero.

When using SIM to describe the predictive performance of the RPE and DDR schemes, smaller SIM values indicate better predictive performance. The results of the SIM comparison are given in Table II, where the SIM of the DDR scheme is better than that of the RPE scheme in almost all cases. In particular, when the block length is longer, such as 4096, the prediction of the RPE-enhanced replay is very poor, while the DDR method is still effective.

From the comparison of the results of the three types of experiments described earlier, it is clear that the DDR approach provides a more reasonable performance prediction than the RPE-enhanced replay method. The advantages of the DDR method compared to RPE-enhanced replay simulation consist of the following reasons: First, the RPE-enhanced replay simulation requires stricter assumptions than the DDR method. It assumes that the RPE is independent of the output of the estimated channel given the transmitted signal so that the RPE can be separated from the OES received signal model. Second, under low-SNR conditions, the performance of the RPE-enhanced replay emulator decreases faster than that of

Authorized licensed use limited to: LEHIGH UNIVERSITY. Downloaded on August 15,2024 at 22:00:01 UTC from IEEE Xplore. Restrictions apply.

This article has been accepted for inclusion in a future issue of this journal. Content is final as presented, with the exception of pagination.

TABLE II
SIM OF DDR AND RPE METHODS FOR QPSK MODULATION/16QAM

Experimental scenario	SIM(DDR,SCM)	SIM(RPE,SCM)	SIM(DDR,OFDM)	SIM(RPE,OFDM)
QPSK, K = 1024, 200 m	0.9608	0.9730	1	1
QPSK, K = 2048, 200 m	1.4066	0.9653	0.9973	0.9990
QPSK, K = 4096, 200 m	11.380	8882445	0.9848	65.1257
QPSK, K = 1024, 1000 m	1.9066	1.9668	0.9360	13.9067
QPSK, K = 2048, 1000 m	1.0129	1.0129	1.0148	1.9966
QPSK, K = 4096, 1000 m	1.4200	14036	6.1205	100480
16QAM, K = 1024, 200 m	3.4641	3.6499	0.9999	1.0093
16QAM, K = 2048, 200 m	2.3840	1.8613	1.7729	7.9429
16QAM, K = 4096, 200 m	1.3283	2192.2	52.476	25567
16QAM, K = 1024, 1000 m	1.1286	1.1683	1.1233	1968.9
16QAM, K = 2048, 1000 m	1.0923	1.0257	2.3377	12358
16QAM, K = 4096, 1000 m	1.2332	1838.1	1.4641	14516

the DDR scheme. This is because the signal caused by the channel estimation error is no longer dominant compared to the ambient noise. Third, under non-Gaussian ambient noise, RPE will have non-Gaussian components that can no longer be characterized by simple second-order statistical properties. In this case, greater computational complexity is required to characterize the non-Gaussian components of RPE; otherwise, the performance prediction of the RPE-enhanced replay emulator will deteriorate significantly. If the RPE is simply calculated by the spatial–temporal correlation matrix and its second-order statistics, then we consider that it can only represent the linear component of the prediction error, while the nonlinear and wide-sense nonstationary components of the channel remain uncompensated. In comparison, the DDR scheme can directly retain the non-Gaussian environmental noise in the channel.

VI. CONCLUSION

In this work, we have extended the DDR techniques originally proposed for coding and modulation schemes to waveform modulation. This allows communication data collected in field experiments to be reused to investigate the performance of different waveform modulation schemes before embarking on the more expensive field experiments. Our proposed DDR method for OFDM and SCM cross evaluation has been evaluated by two field experimental data sets with SCM and OFDM transmissions in the same ocean environment and in adjacent time slots. The receiver uses the same frequency-domain turbo equalizer for all schemes for BER evaluation. A new SIM of the BER performance is also proposed to evaluate the predictive quality of the cross-evaluation methods. The results show that the proposed DDR method is a better cross-evaluation method than the existing RPE-enhanced channel replay method in almost all transmission data sets as the DDR method yields similar BERs as the two original experimental data sets.

REFERENCES

[1] D. B. Kilfoyle and A. B. Baggeroer, "The state of the art in underwater acoustic telemetry," *IEEE J. Ocean. Eng.*, vol. 25, no. 1, pp. 4–27, Jan. 2000.
[2] T. Rappaport, *Wireless Communications: Principles and Practice*, 2nd ed. Englewood Cliffs, NJ, USA: Prentice-Hall, 2002.
[3] C. Xiao, J. Wu, S.-Y. Leong, Y. R. Zheng, and K. B. Letaief, "A discrete-time model for spatio-temporally correlated MIMO WSSUS multipath channels," in *Proc. IEEE Wireless Commun. Netw.*, 2003, pp. 354–358.
[4] M. B. Porter, *The Bellhop Manual and User's Guide: Preliminary Draft*, vol. 260. La Jolla, CA, USA: Heat, Light, Sound Research, Inc., 2011.
[5] J. C. Peterson and M. B. Porter, "Ray/beam tracing for modeling the effects of ocean and platform dynamics," *IEEE J. Ocean. Eng.*, vol. 38, no. 4, pp. 655–665, Oct. 2013.
[6] P. Qarabaqi and M. Stojanovic, "Statistical characterization and computationally efficient modeling of a class of underwater acoustic communication channels," *IEEE J. Ocean. Eng.*, vol. 38, no. 4, pp. 701–717, Oct. 2013.
[7] M. S. Caley and A. J. Duncan, "Wide-band shallow acoustic channel simulation with realistic doppler and delay spreading for 3D evolving rough surfaces," in *Proc. IEEE 3rd Underwater Commun. Netw. Conf.*, 2016, pp. 1–5.
[8] R. Otnes, P. A. van Walree, and T. Jenserud, "Validation of replay-based underwater acoustic communication channel simulation," *IEEE J. Ocean. Eng.*, vol. 38, no. 4, pp. 689–700, Oct. 2013.
[9] P. A. van Walree, F.-X. Socheleau, R. Otnes, and T. Jenserud, "The watermark benchmark for underwater acoustic modulation schemes," *IEEE J. Ocean. Eng.*, vol. 42, no. 4, pp. 1007–1018, Oct. 2017.
[10] G. Deane, J. Preisig, and A. C. Singer, "Making the most of field data to support underwater acoustic communications R&D," in *Proc. 4th Underwater Commun. Netw. Conf.*, 2018, pp. 1–5.
[11] S. Yang, G. B. Deane, J. C. Preisig, N. C. Sevüktekin, J. W. Choi, and A. C. Singer, "On the reusability of postexperimental field data for underwater acoustic communications R&D," *IEEE J. Ocean. Eng.*, vol. 44, no. 4, pp. 912–931, Oct. 2019.
[12] Y. Xue and Y. R. Zheng, "Cross-evaluation of waveform modulation schemes using post-experimental field data for underwater acoustic communications," in *Proc. OCEANS Conf.*, 2022, pp. 1–6.
[13] J. Ling, K. Zhao, J. Li, and M. L. Nordenvaad, "Multi-input multi-output underwater communications over sparse and frequency modulated acoustic channels," *J. Acoust. Soc. Amer.*, vol. 130, no. 1, pp. 249–262, 2011.
[14] J. Zhang and Y. R. Zheng, "Frequency-domain Turbo equalization with soft successive interference cancellation for single carrier MIMO underwater acoustic communications," *IEEE Trans. Wireless Commun.*, vol. 10, no. 9, pp. 2872–2882, Sep. 2011.

Authorized licensed use limited to: LEHIGH UNIVERSITY. Downloaded on August 15,2024 at 22:00:01 UTC from IEEE Xplore. Restrictions apply.

This article has been accepted for inclusion in a future issue of this journal. Content is final as presented, with the exception of pagination.

[15] A. Rafati, H. Lou, and C. Xiao, "Low-complexity soft-decision feedback turbo equalization for MIMO systems with multilevel modulations," *IEEE Trans. Veh. Technol.*, vol. 60, no. 7, pp. 3218–3227, Sep. 2011.
[16] Z. Chen, Y. R. Zheng, J. Wang, and J. Song, "Equivalence of frequency-domain turbo equalization schemes for single-carrier multiple-input–multiple-output systems," *IEEE Trans. Veh. Technol.*, vol. 66, no. 1, pp. 95–106, Jan. 2017.
[17] W. Duan, J. Tao, and Y. R. Zheng, "Efficient adaptive turbo equalization for multiple-input–multiple-output underwater acoustic communications," *IEEE J. Ocean. Eng.*, vol. 43, no. 3, pp. 792–804, Jul. 2018.
[18] B. Ng, C.-T. Lam, and D. Falconer, "Turbo frequency domain equalization for single-carrier broadband wireless systems," *IEEE Trans. Wireless Commun.*, vol. 6, no. 2, pp. 759–767, Feb. 2007.
[19] G. M. Guvensen and A. O. Yilmaz, "A general framework for optimum iterative blockwise equalization of single carrier MIMO systems and asymptotic performance analysis," *IEEE Trans. Commun.*, vol. 61, no. 2, pp. 609–619, Feb. 2013.
[20] X. Qin, F. Qu, and Y. R. Zheng, "Bayesian iterative channel estimation and turbo equalization for multiple-input–multiple-output underwater acoustic communications," *IEEE J. Ocean. Eng.*, vol. 46, no. 1, pp. 326–337, Jan. 2021.
[21] J. Tao, Y. R. Zheng, C. Xiao, and T. Yang, "Robust MIMO underwater acoustic communications using turbo block decision-feedback equalization," *IEEE J. Ocean. Eng.*, vol. 35, no. 4, pp. 948–960, Oct. 2010.
[22] Z. Yang and Y. R. Zheng, "Iterative channel estimation and turbo equalization for multiple-input multiple-output underwater acoustic communications," *IEEE J. Ocean. Eng.*, vol. 41, no. 1, pp. 232–242, Jan. 2016.

Yukang Xue received the bachelor's degree in information engineering from Xi'an Jiaotong University, Xi'an, China, in 2015, and the master's degree in wireless communications and networking in 2018 from Lehigh University, Bethlehem, PA, USA, where he is currently working toward the Ph.D. degree in electrical engineering.

He is also a Teaching Assistant and Research Assistant with Lehigh University. His research interests include various wireless communication technologies, including channel coding, channel estimation, channel equalization, and multicarrier modulation (orthogonal frequency-division multiplexing and orthogonal time–frequency space.)

Xiangzhao Qin (Member, IEEE) received the B.S. degree in underwater acoustic engineering from Harbin Engineering University, Harbin, China, in 2015, and the Ph.D. degree in electrical engineering from Zhejiang University, Zhoushan, China, in 2020.

From 2018 to 2019, he was a Visiting Student with Lehigh University, Bethlehem, PA, USA. From 2020 to 2021, he was the Postdoctoral Fellow with the Department of Marine Technology, University of Haifa, Haifa, Israel. His research interests include underwater acoustic communication and networking and artificial-intelligence-based general signal processing.

Yahong Rosa Zheng (Fellow, IEEE) received the Ph.D. degree in electrical engineering from Carleton University, Ottawa, ON, Canada, in 2002.

She was a Natural Sciences and Engineering Research Council of Canada Postdoctoral Fellow for two years with the University of Missouri, Columbia, MO, USA. From 2005 to 2018, she was with the Faculty of the Department of Electrical and Computer Engineering, Missouri University of Science and Technology, Rolla, MO. In 2018, she joined the Department of Electrical and Computer Engineering, Lehigh University, Bethlehem, PA, USA, as a Professor. Her research interests include underwater and underground Internet of Things and robotics, compressive sensing, wireless communications, and wireless sensor networks.

Dr. Zheng was the recipient of an National Science Foundation Faculty CAREER Award in 2009. She is a Senior Editor for *IEEE Vehicular Technology Magazine*, an Associate Editor for IEEE JOURNAL OF OCEANIC ENGINEERING, and an Associate Editor for three other IEEE journals. She has been a Distinguished Lecturer of the IEEE Vehicular Technology Society since 2015. She has served as a Technical Program Committee Member for many IEEE international conferences.

Authorized licensed use limited to: LEHIGH UNIVERSITY. Downloaded on August 15,2024 at 22:00:01 UTC from IEEE Xplore. Restrictions apply.